The Influence of Pacific SST Variability on the Precipitation over Southern Africa

VASUBANDHU MISRA

Center for Ocean–Land–Atmosphere Studies, Institute of Global Environment and Society, Inc., Calverton, Maryland

(Manuscript received 2 July 2002, in final form 27 November 2002)

ABSTRACT

This study is an analysis of AGCM model results to understand the dynamics of the response of precipitation over southern Africa (SA) to anomalies in the sea surface temperature (SST) over the Pacific Ocean. The pattern of interannual precipitation anomaly over SA and its temporal variations are quite similar in both the ensemble mean of the control (where AGCM is forced with observed SSTs in all ocean basins) and experimental runs (where AGCM is forced with seasonally varying climatological SST over the Pacific Ocean). However, the amplitude of the variability is found to be relatively reduced in the experimental runs. This is shown to be a result of the modulation of the Walker circulation by the variability of Pacific Ocean SST. The regional teleconnection pattern between the dominant mode of SA precipitation variability and SST anomalies over the eastern Indian Ocean is also influenced by the variations in Pacific SST. The nature of the teleconnection between SA precipitation and eastern Indian SST is apparent only when the Pacific SST variability is excluded. This is corroborated from observations as well.

1. Introduction

Many studies have shown a close relationship between the variability of precipitation of the southeastern African region with El Niño–Southern Oscillation (ENSO; Rocha and Simmonds 1997a; Latif et al. 1999; Makarau and Jury 1997; Ropelewski and Halpert 1989; Janowiak 1988). In the austral summer season, Janowiak (1988) found that the rainfall tends to be higher than normal by 10%–25% over equatorial eastern Africa and correspondingly lower in southeast Africa during warm ENSO events. Rocha and Simmonds (1997a) indicate in their study that the strongest relationships are found with the Southern Oscillation index (SOI) leading southeastern Africa rainfall by about 3–6 months. However, they also found a very robust relationship between southeastern African rainfall with the Brandon–Marion index (BMI), which is a measure of changes in the mean sea level pressure over the Indian Ocean. More importantly, they showed that the BMI influences southeastern African rainfall independent of ENSO. Richard et al. (2000) using rain gauge data to show that tropical southern Africa and the SOI were weakly correlated before 1970 but have become significant thereafter. They find that this increase in sensitivity between southern African rainfall and SOI is related to the rise in correlation between SOI and more extensive sea surface temperature anomalies (SSTAs) especially over the southern Indian Ocean. Atmospheric general circulation model (AGCM) simulations from their study indicated that recent ENSO events with warmer SST over the southern oceans lead to a bipolar pattern between southern Africa and the western Indian Ocean. Rocha and Simmonds (1997b) conducted idealized experiments with a coarse-grid AGCM and showed that anomalously warm Indian Ocean SST causes an eastward shift of the Walker circulation from the African subcontinent to the central Indian Ocean. As a result, they indicate the inland moisture flux is reduced and moisture flux convergence over the Indian Ocean is enhanced. Goddard and Graham (1999), using a higher-resolution AGCM with a more sophisticated physics, arrived at similar conclusions. They also found that anomalous SST over the central and eastern Pacific tend to counteract the circulation and precipitation anomalies imposed by the Indian Ocean SSTA over southeastern Africa and the Indian Ocean. Reason and Mulenga (1999), examining nearly 100 yr of observed rainfall and SST datasets, also arrived at similar conclusions that anomalies over the southwestern Indian Ocean significantly impact the rainfall anomalies in eastern South Africa. Latif et al. (1999) using an AGCM showed that the wet anomalies over eastern Africa of December–January–February (DJF) 1997/98 (a strong El Niño year) were a result of contemporaneous warm SSTs over the Indian Ocean. Furthermore, they also showed that El Niño–related SSTA in the eastern Pacific did not directly force this wet anomaly over eastern Africa. It should however be noted that there is a relationship in the SST variability over

Corresponding author address: Dr. Vasubandhu Misra, Center for Ocean–Land–Atmosphere Studies, Institute for Global Environment and Society, Inc., 4041 Powder Mill Road, Suite 302, Calverton, MD 20705.
E-mail: misra@cola.iges.org

the tropical Indian and Pacific Ocean basins (Murtugudde and Busalacchi 1999; Klein et al. 1999; Krishnamurthy and Kirtman 2001). Klein et al. (1999), using satellite and ship data indicate that changes in atmospheric circulation accompanying ENSO modulate the Indian Ocean SST through changes in cloud cover and surface evaporation. One of the most obvious ways to understand the influence of Pacific SST variability on southern Africa (SA) precipitation in a AGCM is to conduct experiments with climatological SST over the Pacific Ocean basin. Unfortunately, AGCM sensitivity studies, including the present one, lack the effect of the simultaneous air–sea coupling as in a coupled ocean–atmosphere model. Ideally, these sensitivity studies should be conducted with coupled ocean–atmosphere models. However, the errors due to climate drift in the coupled Center for Ocean–Land–Atmosphere studies (COLA) model is so large (Kirtman et al. 2002) that it makes it unsuitable for analyzing such regional teleconnection patterns.

Recent modeling studies of Goddard and Graham (1999) and Latif et al. (1999) have shown the importance of the Indian Ocean SSTA on precipitation variability over SA. We were initially motivated to see how in another (COLA) AGCM, SA precipitation variability responds to SSTA in the Pacific Ocean. Figures 1a,b show the climatological ensemble mean of DJF precipitation from the control integration and its difference with an experimental run of the COLA AGCM over an 18-yr period between 1979 and 1997. The model is described in the following section. In the control runs, observed SST is prescribed in all ocean basins while, in the experimental runs observed SST is replaced with seasonally varying climatological SST over the entire Pacific Ocean basin. There is enhanced (reduced) DJF precipitation over south-central (southeastern) Africa in the control relative to the experiment. Henceforth, we shall refer to this region of sensitivity as SA. The difference in Fig. 1b is nearly 25% of the climatological mean over SA in Fig. 1a, which suggests that SA precipitation variability is significantly influenced by SST over the Pacific Ocean. One of the goals of this paper is to understand this response of the SA precipitation to variability of SST over the Pacific Ocean. In this study we will also further explore the observed teleconnection of SA precipitation variability with Indian Ocean SSTA. In the following section we describe the datasets used in this study followed by a brief description of the COLA AGCM adopted in this study, which is followed by the design of experiments. The results are discussed in section 5 followed by concluding remarks.

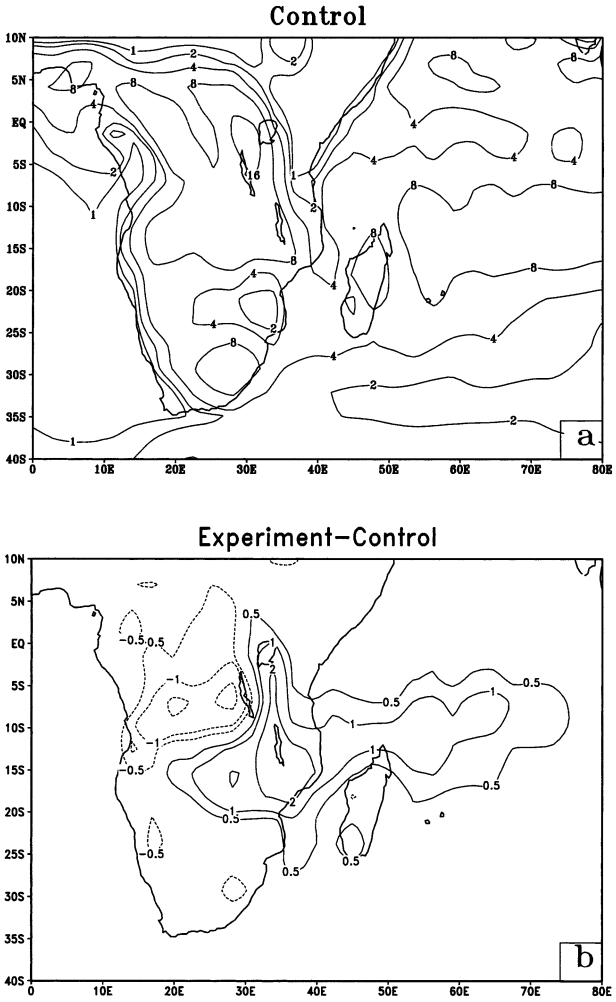

FIG. 1. (a) Mean DJF precipitation from the control run and (b) its difference from the experimental run. The units are mm day^{-1}.

2. Datasets

In this study we have validated some of the model results with available observations. We have used the Climate Prediction Center (CPC) Merged Analysis of Precipitation (CMAP), which follows Xie and Arkin (1996), to compare with the COLA AGCM–generated precipitation. CMAP produces monthly analyses of global precipitation in which observations from rain gauges are merged with precipitation estimates from several satellite-based algorithms. The precipitation analyses is on a 2.5° × 2.5° latitude–longitude grid and is available over the time period from January 1979 to the present. The SST is obtained from the monthly mean of the Hadley Centre Sea Ice and Sea Surface Temperature dataset (HadISST; Parker et al. 1999). This HadISST is an improved SST analysis over the Global Sea Ice and SST dataset (GISST; Rayner et al. 1996) and is computed on a 1° × 1° grid from 1870 to the present. This HadISST is used to analyze the observed teleconnection patterns of SA precipitation with global SSTA. The zonal wind from the National Centers for Environmental Prediction–National Center for Atmospheric Research (NCEP–NCAR) reanalysis (Kalnay et

al. 1996) is used for the examination of the Walker circulation.

3. Model description

The AGCM used in this study is version 2.2 of the COLA global spectral model at T42 (~2.5°) horizontal resolution and 18 levels (COLA–AGCM). This version of the model has the dynamical core of the NCAR Climate Community Model version 3 (CCM3) described in Kiehl et al. (1998). The dependent variables of the model are spectrally treated except the moisture variable, which is advected using the semi-Lagrangian technique. The parameterization of deep convection is the relaxed Arakawa–Schubert scheme (Moorthi and Suarez 1992). The subgrid-scale exchange of heat, momentum, and moisture is accomplished via a turbulent closure scheme, level 2.0 (Mellor and Yamada 1982). The diagnostic cloud fraction and optical properties are similar to CCM3 (Kiehl et al. 1998) and are described in DeWitt and Schneider (1997). The terrestrial and shortwave radiation follows Harshvardhan et al. (1987) and Davies (1982), respectively. A fourth-order horizontal diffusion is applied to all variables except the moisture variable. A mean surface orography (Fennessy et al. 1994) is used to represent surface elevation. Dry convective adjustment and gravity wave drag are not invoked in the model integrations. The shallow convective scheme of Tiedtke (1984) is employed in the model. The atmospheric model is coupled to the Simplified Simple Biosphere model (SSiB) documented in Xue et al. (1991, 1996).

The surface boundary condition of SST is obtained from HadISST. The soil moisture fields are obtained from a 2-yr climatology of the Global Soil Wetness Project (Dirmeyer and Zeng 1999).

4. Design of experiments

A set of six control integrations were conducted using different initial conditions starting from 0000 UTC 1 December 1978 to 0000 UTC 1 January 1997 with the COLA AGCM. The initial conditions were obtained as restart files of COLA AGCM generated 7 days apart (so that they are synoptically independent) with the time reset to the initial date (Misra et al. 2003; Kirtman et al. 2001) of the model integration. A set of six experimental runs were made using seasonally varying climatological SST over the Pacific Ocean basin and observed SST as in the control run over the rest of the ocean basins. The atmospheric and land surface initial conditions for these six experimental runs were borrowed from the control integrations.

A more conventional way of designing these experiments would have been to describe a control AGCM integration forced with climatological SST everywhere and an experimental integration with observed SST variability over the Pacific. However, since we are examining linear responses to SSTA, either set of experiments should not change the conclusions of this study. Furthermore, the design of experiments adopted in this study enables us to also examine the role of Pacific SSTA on the modulation of the teleconnection pattern between Indian Ocean SSTA and SA precipitation variability.

5. Results

In the following discussion results from the ensemble mean over the six members are presented for both the control and the experimental runs. Furthermore, the focus of this paper is on the DJF season when the response of the precipitation over SA to Pacific SST variability is largest in the model integrations (not shown) and in observations (Janowiak 1988).

The COLA AGCM generates reasonable simulations of the present climate (Dirmeyer et al. 2002) and is comparable to other AGCMs. The COLA AGCM is also a participant model in the Atmospheric Model Intercomparison Project (AMIP; Gates et al. 1999). Gates et al. (1999) show that the COLA AGCM has comparable skill relative to other models in AMIP in simulating rainfall, outgoing longwave radiation, sea level pressure, surface air temperature, and ocean surface heat flux. The variability of the model, notwithstanding the systematic errors of the control model, is reasonable. In Figs. 2a,b we show the composite mean precipitation from La Niña years (listed in Table 1) and its difference from the corresponding mean from El Niño events in the control run. The corresponding figures from observations based on CMAP are shown in Fig. 3. There is a huge drift in the COLA AGCM over SA with the model precipitating in excess relative to the observations. However, the magnitudes of the anomalies are comparable. The anomaly over southeastern Africa in the model is shifted farther north relative to observations and the positive anomaly is larger in magnitude and extent. Furthermore, the anomalies over southeastern Africa are oriented northeast–southwest, while, observations indicate a northwest–southeast orientation. However, despite these discrepancies in the model simulation, the signs of the anomalies and their amplitudes over south-central and southeastern Africa are quite consistent with observations. This anomalous structure implies that in warm (cold) episodes of ENSO south-central Africa receives more (less) than normal rainfall, while in southeastern Africa it receives less (more) than normal rainfall. This teleconnection pattern is also consistent with the observational studies of Janowiak (1988) and Ropelewski and Halpert (1989).

As mentioned earlier, Fig. 1 depicts the mean difference of precipitation for DJF between the control and experimental AGCM integrations. This difference pattern is similar to the ENSO variability pattern shown in Fig. 2a. This result is rather obvious because ENSO-related SSTAs dominate the interannual variability in the Pacific Ocean.

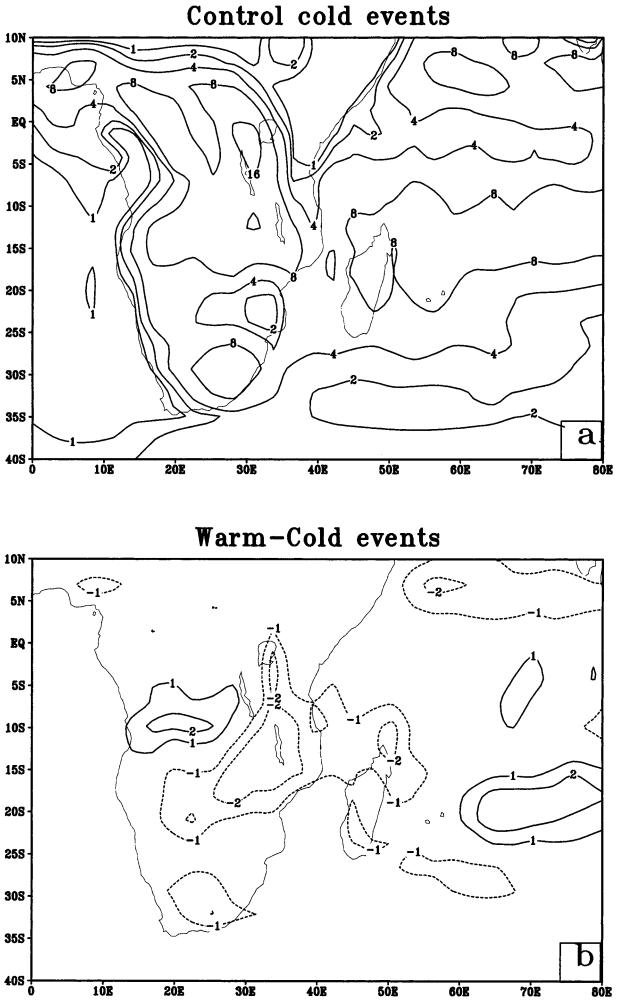

FIG. 2. (a) The precipitation averaged over cold (La Niña) events (see Table 1) and (b) its difference from warm (El Niño) events. The units are mm day^{-1}.

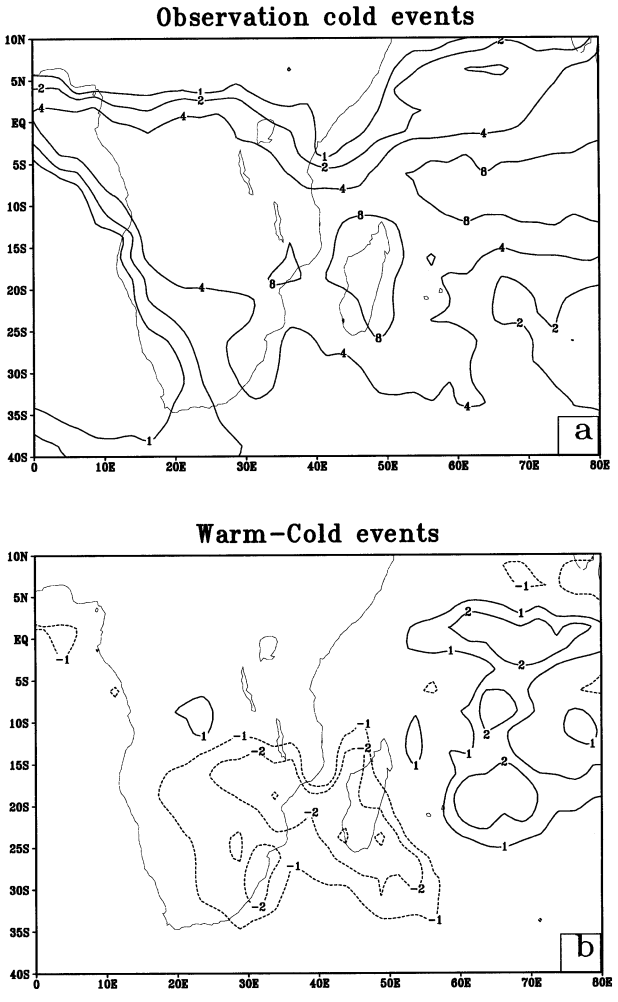

FIG. 3. Same as Fig. 2 but from observations based on CMAP.

An empirical orthogonal function (EOF) analysis was performed on the precipitation obtained from the control and the experimental runs. The domain for conducting this EOF analysis is identical to that shown in Fig. 1.

TABLE 1. El Niño and La Niña years chosen for plotting Figs. 2 and 3 along with the amplitude of DJF Niño-3 (5°S–5°N, 90°–150°W) anomalies (calculated from a 50-yr climatology covering a period from 1948 to 1998 using the Hadley Centre monthly mean SST dataset).

Year	Event	DJF Niño-3 anomalies (°C)
1982/83	El Niño	2.45
1986/87	El Niño	1.142
1991/92	El Niño	1.579
1994/95	El Niño	0.994
1983/84	La Niña	−0.512
1984/85	La Niña	−1.159
1988/89	La Niña	−1.353
1995/96	La Niña	−0.579

The variance explained by the first seven EOFs are shown in Table 2 for both the control and the experimental means. We see that the first EOF explains the most variance in both model runs. In addition, there is a clear separation in the variance explained from the first EOF and the remainder of the EOFs, establishing that the first EOF is the most dominant pattern of variability in both the control and the experiment. In Figs. 4a,b we depict the spatial pattern of the first EOF and

TABLE 2. Percent variance explained by the first seven EOFs of precipitation over southeastern Africa for both the control and experiment.

EOF	Control	Experiment
1	47.53	42.09
2	12.57	13.02
3	7.17	8.72
4	5.74	6.28
5	4.92	5.24
6	3.46	4.55
7	3.19	3.5

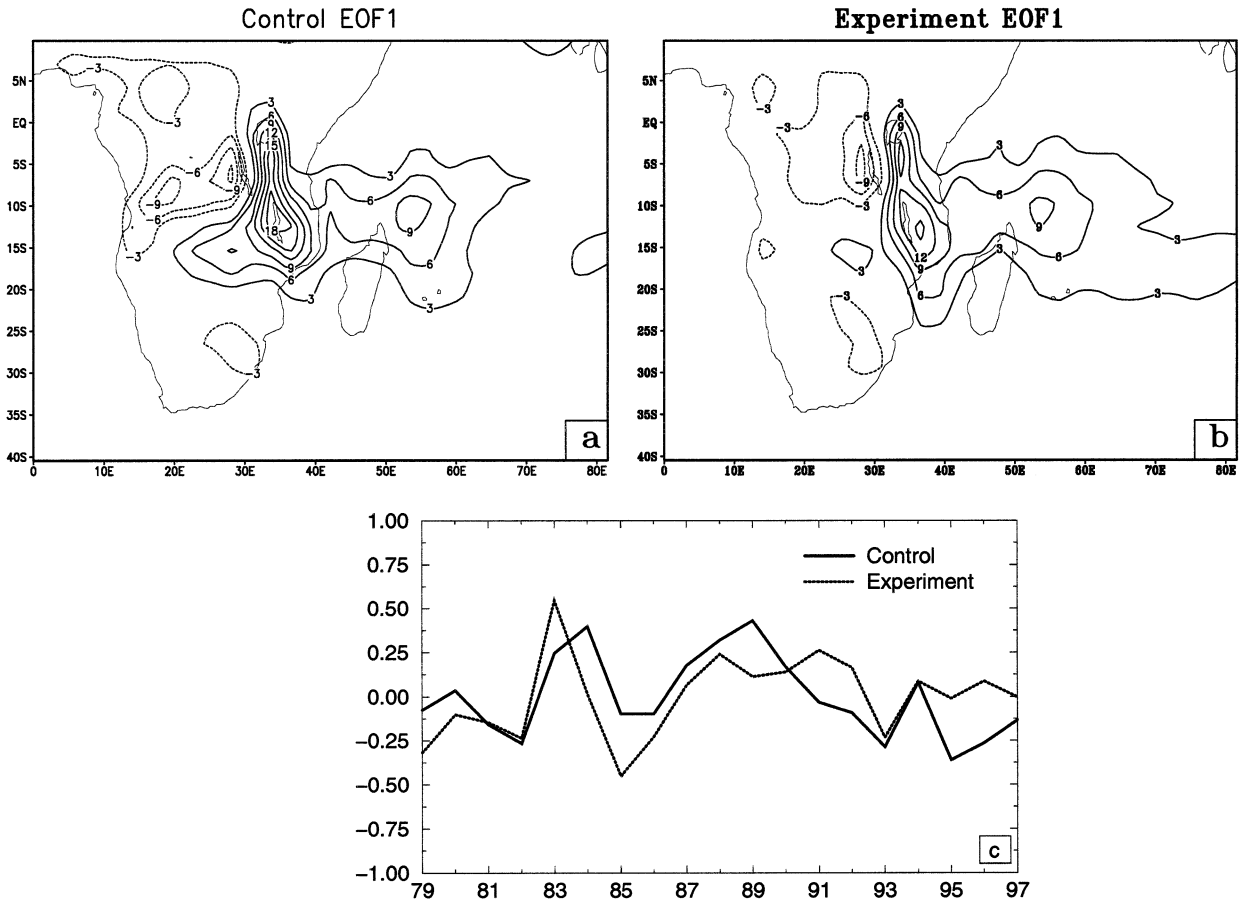

FIG. 4. The spatial pattern of the first EOF (EOF1) for DJF precipitation from the (a) control, (b) experiment, and (c) the corresponding time coefficients of the first EOF. Units are arbitrary.

in Fig. 4c its corresponding temporal coefficients [principal component (PC)] from the control and the experiment, respectively. The EOFs from the ensemble means of the two models depict comparable spatial patterns and temporal variations. Furthermore, the spatial pattern of EOF1 in Figs. 4a,b bears fairly close resemblance to the ENSO variability pattern of precipitation from the control model shown in Fig. 2a. It is also apparent that the amplitude of the EOF pattern is smaller in the experimental run (Fig. 4b) compared to the control run (Fig. 4a). Although EOF analysis is domain dependent (Richman 1986), EOF1 in this study clearly picks the dominant interannual variability component of precipitation over SA. This analysis thus far suggests that the spatial structure and temporal variation of the dominant variability of SA precipitation is somewhat independent of the Pacific Ocean SST variability. But in these model integrations we also find that the amplitude of the dominant SA precipitation variability is modulated by the Pacific Ocean SST variability. However, it should be noted that these results may be unique to AGCM integrations with prescribed SST, as these ignore any existing relationship between Indian and Pacific Ocean SST variability, which is currently being debated (Krishnamurthy and Kirtman 2001; Saji et al. 1999).

In Figs. 5a,b we have plotted the statistically significant correlations (at the 90% confidence interval) of the time coefficients in Fig. 4c from the control and experimental runs with global SST distribution for September–October–November, (SON) respectively. It should be mentioned that the SST leads the principal component of the first EOF of precipitation. The strongest correlations in the control run were found with SON SST. Krishnamurthy and Kirtman (2001) have shown that the dominant variability pattern of the dipole structure over the Indian Ocean appears most strongly in the SON season in congruence with anomalies in the tropical Pacific. It is seen from these figures that the SA precipitation from the experimental ensemble mean, unlike the control model, correlates with the eastern Indian Ocean SSTA rather strongly. This also suggests that the regional teleconnections have been modulated by Pacific SST variability, which has led to the change in correlation patterns between Figs. 5a and 5b. We conducted a similar analysis (not shown) with precipitation over south-central and southeastern Africa separately with

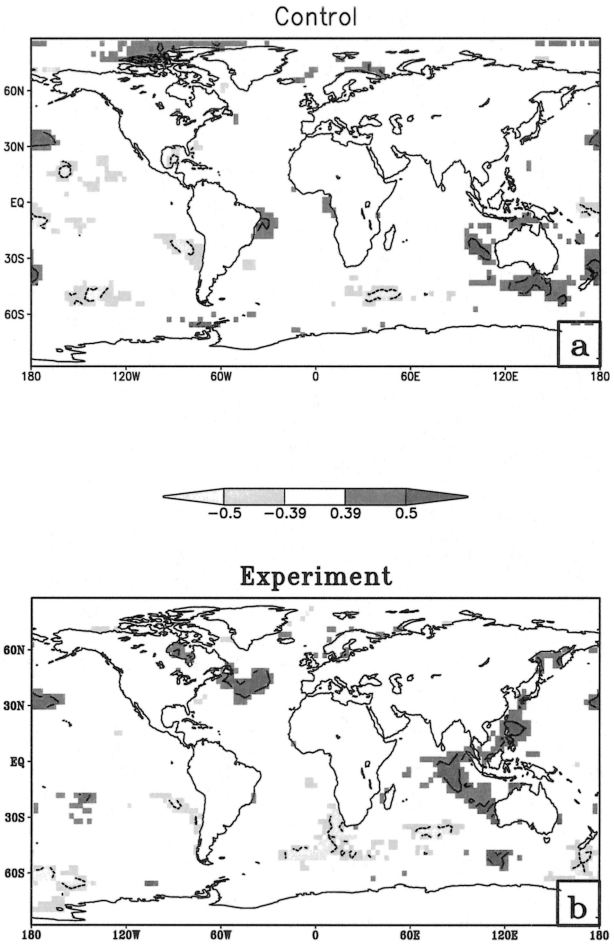

FIG. 5. The correlation of the time coefficient of the first EOF of precipitation (shown in Fig. 4c) with global SST (HadISST) for the SON season from the (a) control and the (b) experiment. The SST leads the principal component. Only significant values at the 90% confidence interval according to a *t* test are plotted.

global SST and arrived at similar relationships (with teleconnection patterns that were orthogonal to each other). Similar, albeit weaker correlations were found when contemporaneous SST was used. We investigated this result further using observed DJF mean precipitation (CMAP). The observed precipitation time series from 1979 to 1997 was obtained by averaging over a domain between 30°–15°S and 30°–40°E where the ENSO response was relatively large (Fig. 3b). This time series when correlated with global SON SST (with a lag of one season as in Fig. 5a) showed no significant (at the 90% confidence interval) correlation with eastern Indian Ocean. However, when only weak ENSO years (see Table 3) with Niño-3 anomalies less than 0.4σ were used for this correlation analysis then the telconnection between precipitation over southeastern Africa and the eastern Indian Ocean appears the at 90% confidence interval as shown in Fig. 6. This is reasonably similar to the correlation pattern that was obtained from the experimental run in Fig. 5b. Although, the correlations

TABLE 3. The years of weak ENSO events for plotting Fig. 6 along with the amplitude of DJF Niño-3 anomalies (calculated from a 50-yr climatology covering a period from 1948 to 1998 using HadISST).

Year	Event	DJF Niño-3 anomalies (°C)
1978/79	Weak ENSO	0.109
1980/81	Weak ENSO	−0.338
1981/82	Weak ENSO	0.310
1989/90	Weak ENSO	−0.076
1990/91	Weak ENSO	0.172
1993/94	Weak ENSO	−0.012

over the Indian Ocean in the model runs are slightly shifted to the west compared to Fig. 5 it should be noted that in observations weak ENSO events are included while in the AGCM experiments the variability of Pacific SST has been completely shut off.

In Fig. 7a we show the mean DJF velocity potential and divergent wind component at 200 hPa from the control ensemble mean. The divergence over the warm pool region of the Pacific Ocean, Indonesia, and the central Indian Ocean are associated with low-level convergence, upward motion, and large precipitation amounts, which are characteristic of the region. This ascending cell also represents one of the main cells of the east–west Walker circulation. This planetary-scale Walker circulation extends eastward over the eastern Pacific and Atlantic Oceans, and westward over the western Indian Ocean and northern Africa with upper-level convergence centers that represent the descending cells of the Walker circulation associated with low-level divergence and weak precipitation.

For comparison the mean difference of the velocity potential and the divergent component of the wind at

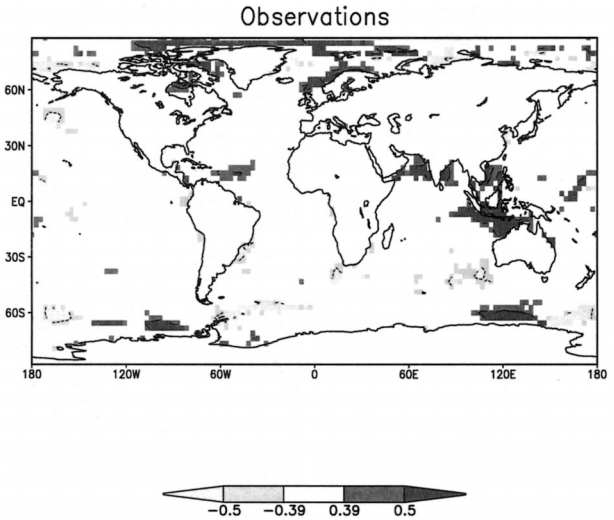

FIG. 6. The correlation of the time series of area-averaged DJF precipitation from CMAP and SON HadISST for weak ENSO years (see Table 3). The SST leads the observed precipitation. Only significant values at the 90% confidence interval according to a *t* test are plotted.

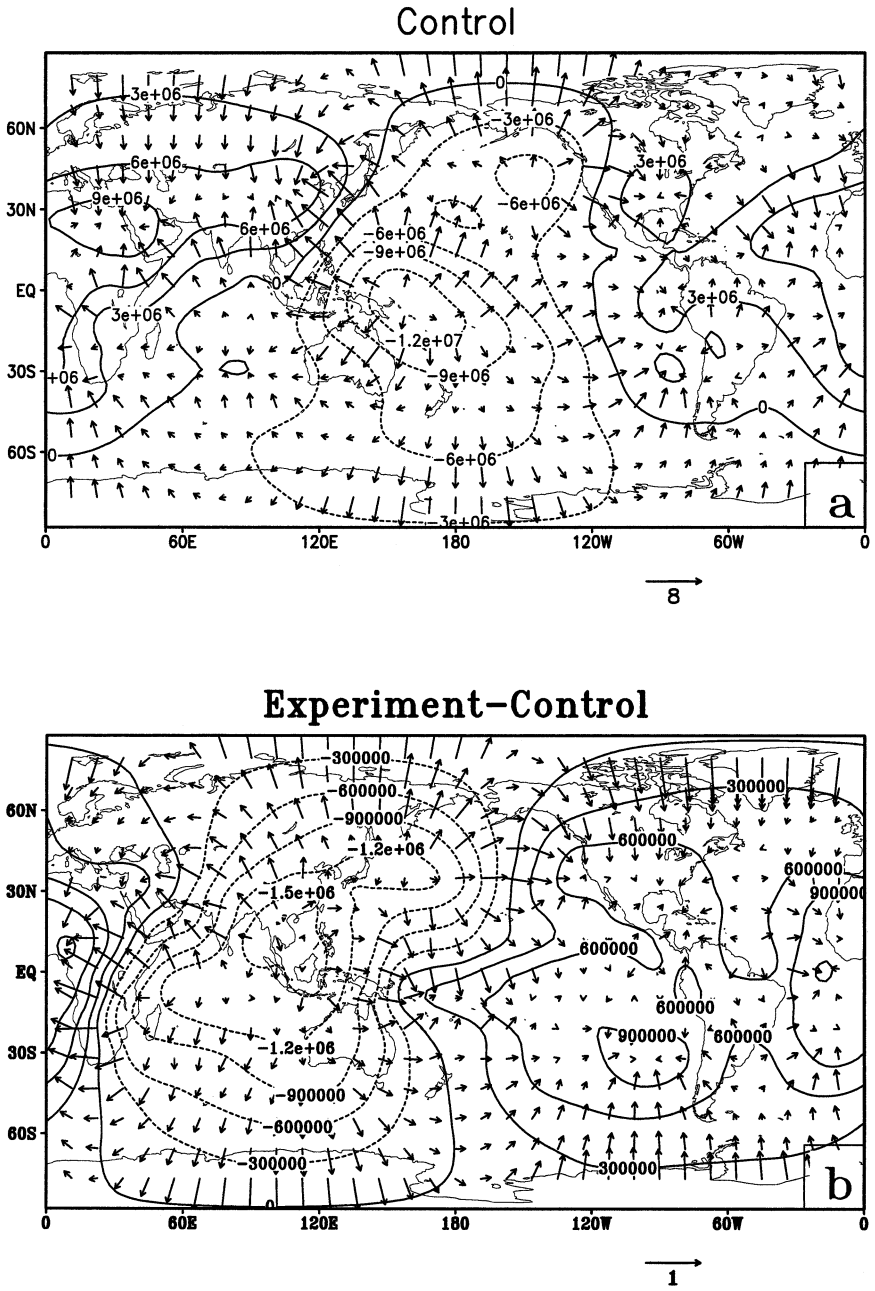

FIG. 7. (a) Velocity potential and divergent wind at 200 hPa for DJF from the control mean. The isopleth interval is 3.0×10^6 m^2 s^{-1}. (b) The mean difference for DJF of velocity potential and divergent wind at 200 hPa between the control and experimental mean. The isopleth interval is 3.0×10^5 m^2 s^{-1}. The unit of the wind vectors is m s^{-1}.

200 hPa between the control and experimental ensemble mean for DJF are plotted in Fig. 7b. It is clearly seen from Fig. 7b that in the absence of Pacific Ocean SST variability, the upper-level divergence (which is part of the ascending cell) of the mean Walker circulation over the eastern Indian Ocean and Indonesia is enhanced, while it diminishes over the western Pacific Ocean. Likewise, the upper-level convergence (representing the descending cells) of the mean Walker circulation in the experimental run over the eastern Pacific and the Atlantic and western and central Africa is relatively enhanced but diminished over the Asian monsoon region and eastern Africa. Since the amplitude of the interannual variability of SSTA over the eastern Indian Ocean is much smaller than that in the tropical Pacific Ocean, its impact is seen much more in the variability

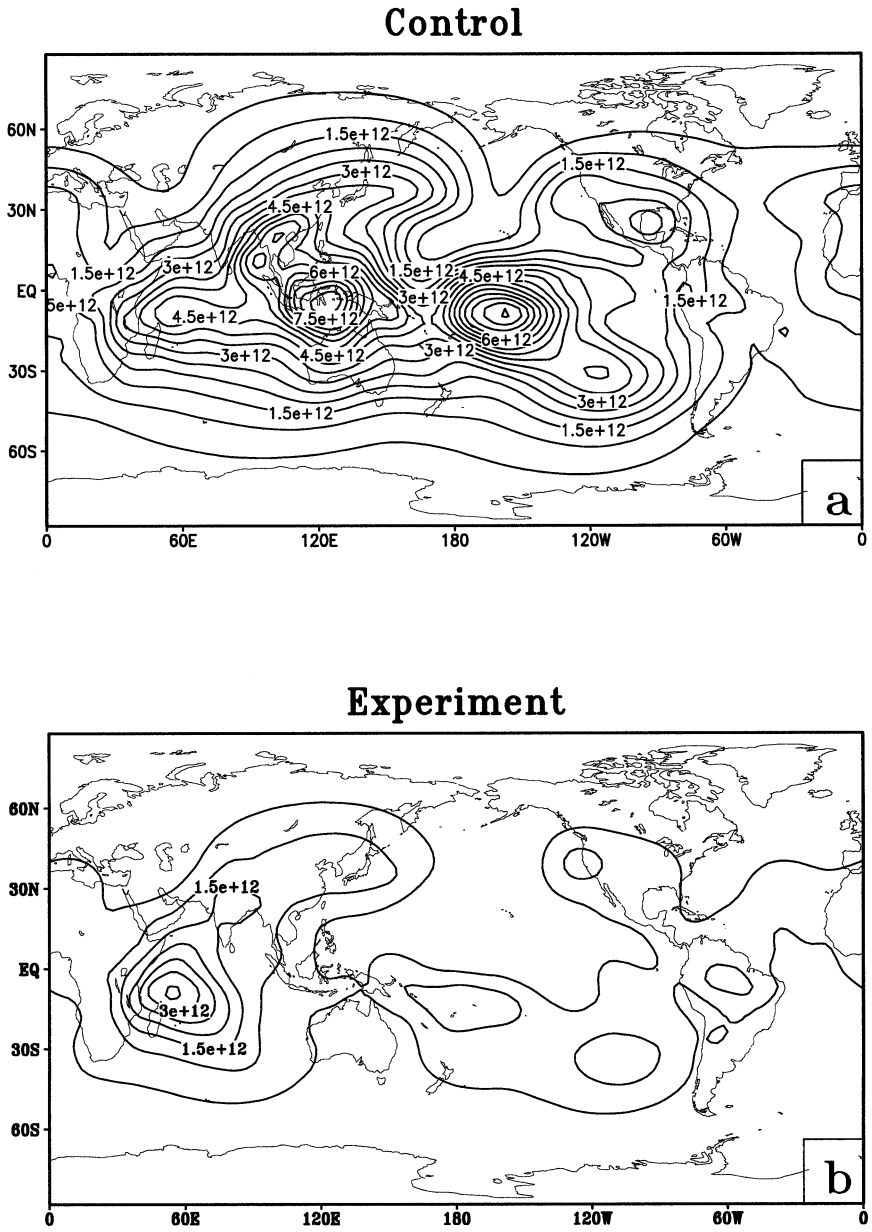

FIG. 8. Variance of velocity potential at 200 hPa for DJF from the (a) control and (b) experimental means. The isopleth interval is 5.0×10^{11} m^4 s^{-2}.

of the circulation field in the experimental run rather than in the control. This is shown in Figs. 8a,b which depict the variance of the velocity potential (χ) for DJF from the control and experimental runs. It is seen that the variability of the χ field in the control run (Fig. 8a) is much more than that in the experimental run especially along eastern Africa and the eastern Indian Ocean. This is consistent with the smaller amplitude of SA precipitation variability in the experimental run.

These sets of AGCM experiments suggest that the mean Walker circulation shifts westward in the absence of Pacific Ocean SST variability, which enhances the teleconnection of the SA precipitation variability with the eastern Indian and southeastern Atlantic Oceans and diminishes the amplitude of the variability of the SA precipitation. However, the spatial structure and the temporal variability of the dominant precipitation pattern over SA is largely unaffected by the absence of Pacific SST variability.

To understand the connection of the Walker circulation to the SA precipitation variability in the control run we regressed the area-averaged DJF precipitation obtained from a domain 20°–5°S and 30°–40°E (southeastern Africa) to the zonal wind anomalies averaged

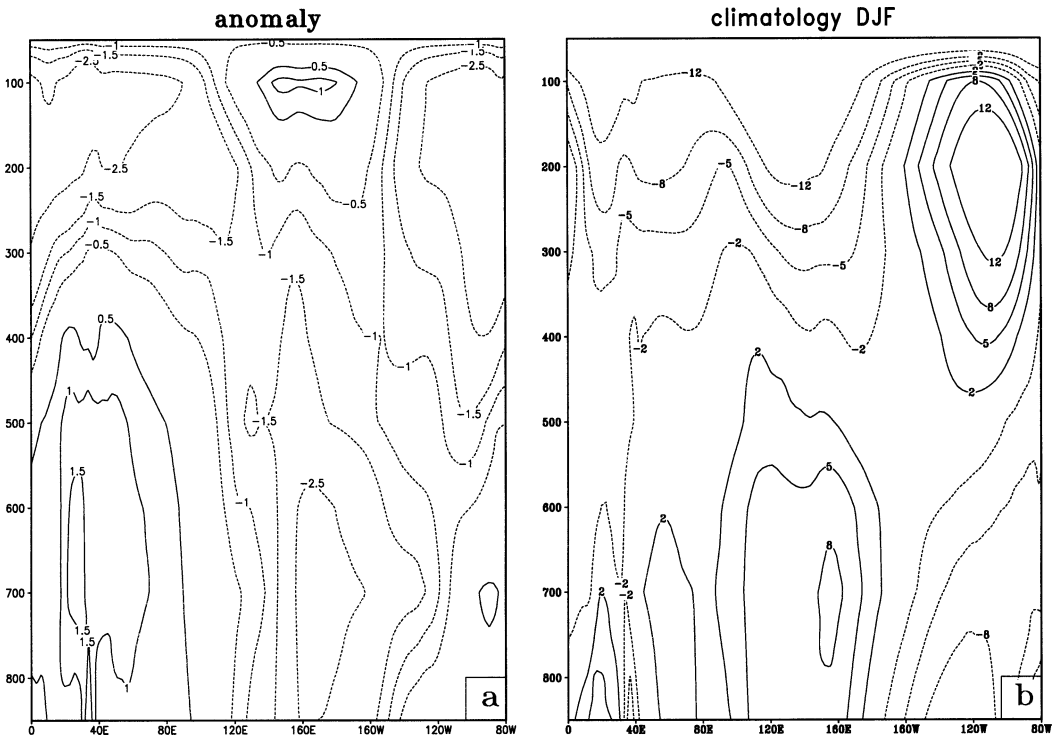

FIG. 9. (a) The linear regression of the southeastern African rainfall anomaly on the control AGCM zonal wind anomaly averaged between 0° and 10°S and (b) the climatology of the zonal wind averaged between 0° and 10°S from the control AGCM. (Units: m s^{-1}). The ordinate is pressure levels in hPa.

between 0° and 10°S. Here we are using this meridionally averaged equatorial zonal wind as a proxy for the Walker circulation over the Indo-Pacific region. In Fig. 9a we show the vertical structure of the response of the zonal wind anomaly to an eastern African precipitation anomaly of 2 mm day^{-1} from the control run. The corresponding climatology of the equatorial zonal wind from the control run is plotted in Fig. 9b. In the control run it is seen that a positive anomaly over southeastern Africa generally enhances the Walker circulation over both the Indian and Pacific Oceans except for the westerlies in the mid- to upper troposphere in the eastern Pacific, which is weakened slightly. This relationship is maintained in the experimental run as shown in Figs. 10a,b especially over eastern Africa and the western Indian Ocean. However, the anomalous response of the equatorial zonal wind is weaker in the experimental run (Fig. 10a) than in the control run (Fig. 9a) over the western Indian and Pacific Oceans. We also conducted a similar analysis with CMAP anomalies and NCEP–NCAR reanalysis equatorial zonal winds and found a similar relationship; that is, during weak ENSO years the response of the equatorial zonal wind anomaly over the Pacific to southeast African preciptation is weaker (not shown).

6. Conclusions

In this study we have analyzed the influence of Pacific Ocean SST variability on precipitation over southern Africa (SA). The control ensemble mean was compared with an experimental ensemble mean wherein the seasonally varying climatological SST over the entire Pacific Ocean was prescribed. The difference in these experiments shows that the temporal variation and the spatial structure of the first EOF of preciptiation over SA in the control run is somewhat independent of SST variability over the Pacific Ocean. However, the amplitude of this variability of the SA precipitation is reduced by the absence of Pacific Ocean SST variability. We find that this response of the SA precipitation is associated with the westward shift of the rising cell of the Walker circulation in the experimental run relative to the control. In the experimental run the ascending cell of the Walker circulation is centered farther westward over the eastern Indian Ocean. This results in the reduction of variability of the Walker circulation in the experimental run since the variations of the Indian Ocean SSTA are much smaller than that of Pacific Ocean SST variability. This shift of the Walker circulation also enhances the correlation between SA precipitation and eastern Indian Ocean SSTA. This relationship is confirmed with observations.

Therefore, it may be concluded that in the COLA AGCM the Pacific Ocean SST variability interferes with the amplitude of the SA precipitation and its correlation with the eastern Indian Ocean SSTA by modulating the large-scale Walker circulation.

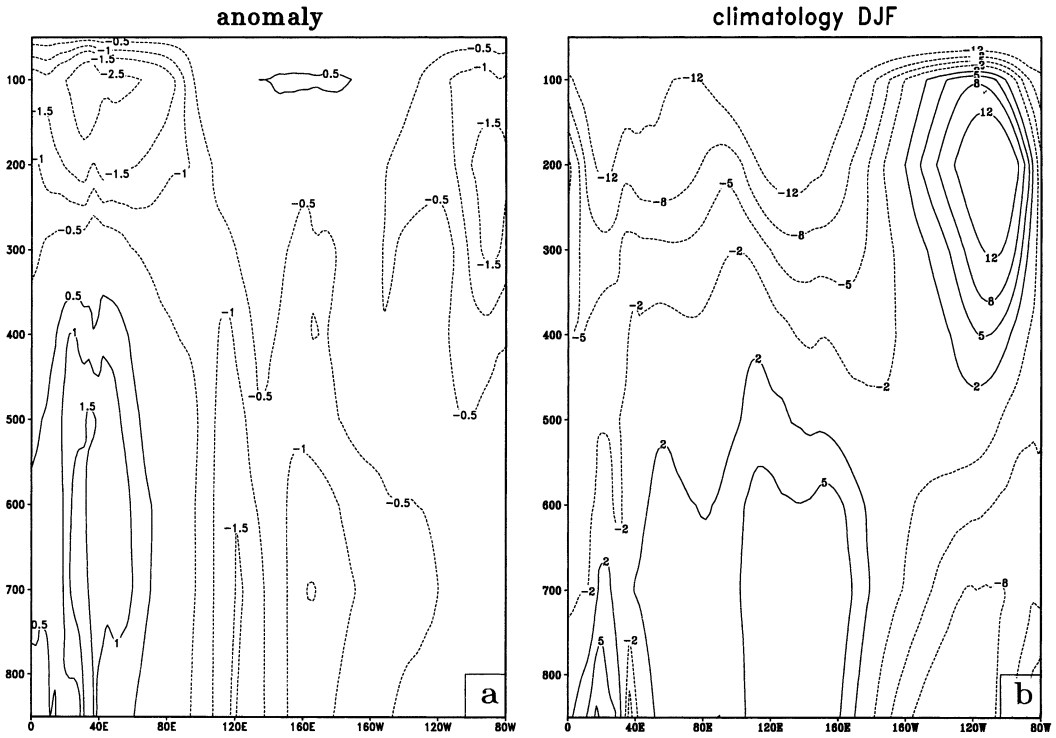

FIG. 10. Same as Fig. 9 but from the experimental run.

Acknowledgments. I would like to thank Paul Dirmeyer for providing the SST datasets for the experimental run. The author acknowledges the support of Paul Dirmeyer and Ben Kirtman to pursue this study. This project was supported by NASA Grant NAG5-8416 and NOAA Grant NA86GP0258.

REFERENCES

Davies, R., 1982: Documentation of the solar radiation parameterization in the GLAS climate model. NASA Tech. Memo. 83961, 57 pp.

DeWitt, D. G., and E. K. Schneider, 1997: The Earth radiation budget as simulated by the COLA GCM. COLA Rep. 35, 39 pp. [Available from COLA, 4041 Powder Mill Rd., Suite 302, Calverton, MD 20705.]

Dirmeyer, P. A., and F. J. Zeng, 1999: Precipitation infiltration in the Simplified SiB land surface scheme. *J. Meteor. Soc. Japan,* **77,** 291–303.

——, M. J. Fennessy, and L. Marx, 2002: Near surface boreal summer climate as simulated by three general circulation models. COLA Rep. 100, 39 pp. [Available from COLA, 4041 Powder Mill Rd., Suite 302, Calverton, MD 20705.]

Fennessy, M. J., and Coauthors, 1994: The simulated Indian monsoon: A GCM sensitivity study. *J. Climate,* **7,** 33–43.

Gates, W. L., and Coauthors, 1999: An overview of the results of the Atmospheric Model Intercomparison Project (AMIP I). *Bull. Amer. Meteor. Soc.,* **80,** 29–55.

Goddard, L., and N. E. Graham, 1999: Importance of the Indian Ocean for simulating rainfall anomalies over eastern and southern Africa. *J. Geophys. Res.,* **104,** 19 099–19 116.

Harshvardhan, R. Davies, D. A. Randall, and T. G. Corsetti, 1987: A fast radiation parameterization for atmospheric circulation models. *J. Geophys. Res.,* **92** (D1), 1009–1016.

Janowiak, J., 1988: An investigation of interannual rainfall variability in Africa. *J. Climate,* **1,** 240–255.

Kalnay, E., and Coauthors, 1996: The NCEP/NCAR 40-Year Reanalysis Project. *Bull. Amer. Meteor. Soc.,* **77,** 437–471.

Kiehl, J. T., J. J. Hack, G. Bonan, B. A. Boville, D. L. Williamson, and P. J. Rasch, 1998: The National Center for Atmospheric Research Community Climate Model: CCM3. *J. Climate,* **11,** 1131–1149.

Kirtman, B. P., D. A. Paolino, J. L. Kinter, and D. M. Straus, 2001: Impact of tropical subseasonal SST variability on seasonal mean climate simulations. *Mon. Wea. Rev.,* **129,** 853–868.

——, Y. Fan, and E. K. Schneider, 2002: The COLA global coupled and anomaly coupled ocean–atmosphere GCM. *J. Climate,* **15,** 2301–2320.

Klein, S. A., B. J. Soden, and N.-C. Lau, 1999: Remote sea surface temperature variations during ENSO: Evidence for a tropical atmospheric bridge. *J. Climate,* **12,** 917–932.

Krishnamurthy, V., and B. P. Kirtman, 2001: Variability of the Indian Ocean: Relation to monsoon and ENSO. COLA Rep. 107, 39 pp. [Available from COLA, 4041 Powder Mill Rd., Suite 302, Calverton, MD 20705.]

Latif, M., D. Dogmmenget, M. Dima, and A. Grotzner, 1999: The role of Indian Ocean sea surface temperature in forcing East African rainfall anomalies during December–January 1997/98. *J. Climate,* **12,** 3497–3504.

Makarau, A., and M. R. Jury, 1997: Predictability of Zimbabwe summer rainfall. *Int. J. Climatol.,* **17,** 1421–1432.

Mellor, G. L., and T. Yamada, 1982: Development of a turbulence closure model for geophysical fluid processes. *Rev. Geophys. Space Phys.,* **20,** 851–875.

Misra, V., P. A. Dirmeyer, and B. P. Kirtman, 2003: Dynamic downscaling of seasonal simulations over South America. *J. Climate,* **16,** 103–117.

Moorthi, S., and M. J. Suarez, 1992: Relaxed Arakawa–Schubert: A parameterization of moist convection for general circulation models. *Mon. Wea. Rev.,* **120,** 978–1002.

Murtugudde, R., and A. J. Busalacchi, 1999: Interannual variability of the dynamics and thermodynamics of the Indian Ocean with relevance to 1997–1998. *J. Geophys. Res.,* **104,** 3295–3306.

Parker, D. E., N. A. Rayner, E. B. Horton, and C. K. Folland, 1999: Development of the Hadley Center sea ice and sea surface temperature data sets (HADISST). *Proc. WMO Workshop on Advances in Marine Climatology—CLIMAR99,* Vancouver, BC, Canada, WMO, 194–203.

Rayner, N. A., E. B. Horton, D. E. Parker, C. K. Folland, and R. B. Hackett, 1996: Version 2.2 of the global sea-ice and sea surface temperature data set, 1903–1994. Climate Research Tech. Note CRTN 74, 43 pp. [Available from Met Office, London Road, Bracknell, Berkshire RG12 2SZ, United Kingdom.]

Reason, C. J. C., and H. Mulenga, 1999: Relationships between South African rainfall and SST anomalies in the southwest Indian Ocean. *Int. J. Climatol.,* **19,** 1651–1673.

Richard, Y., S. Trzaska, P. Roucou, and M. Rouault, 2000: Modification of the southern African rainfall variability/ENSO relationship since the late 1960s. *Climate Dyn.,* **16,** 883–895.

Richman, M. B., 1986: Review article rotation of principal components. *Int. J. Climatol.,* **6,** 293–335.

Rocha, A., and I. Simmonds, 1997a: Interannual variability of southeastern African summer rainfall. Part I: Relationships with air–sea interaction processes. *Int. J. Climatol.,* **17,** 235–265.

——, and ——, 1997b: Interannual variability of southeastern African summer rainfall. Part II: Modelling the impact of sea-surface temperatures on rainfall and circulation. *Int. J. Climatol.,* **17,** 267–290.

Ropelewski, C. F., and M. S. Halpert, 1989: Precipitation patterns associated with the high index phase of the Southern Oscillation. *J. Climate,* **2,** 268–284.

Saji, N. H., B. N. Goswami, P. N. Vinayachandrana, and T. Yamagata, 1999: A dipole mode in the tropical Indian Ocean. *Nature,* **401,** 360–363.

Tiedtke, M., 1984: The effect of penetrative cumulus convection on the large-scale flow in a general circulation model. *Beitr. Phys. Atmos.,* **57,** 216–239.

Xie, P., and P. Arkin, 1996: Analysis of global monthly precipitation using guage observations, satellite estimates, and numerical model predictions. *J. Climate,* **9,** 840–858.

Xue, Y.-K., P. J. Sellers, J. L. Kinter, and J. Shukla, 1991: A Simplified Biosphere model for global climate studies. *J. Climate,* **4,** 345–364.

——, F. J. Zeng, and C. A. Schlosser, 1996: SSiB and its sensitivity to soil properties: A case study using HAPEX-Mobilhy data. *Global Planet. Change,* **13,** 183–194.